

Supporting Information for

A size dependent sodium storage mechanism in  
 $\text{Li}_4\text{Ti}_5\text{O}_{12}$  investigated by a novel  
characterization technique combining *in situ* X-  
ray diffraction and chemical sodiation

Xiqian Yu<sup>1 ‡</sup>, Huilin Pan,<sup>2 ‡</sup> Wang Wan<sup>1</sup>, Chao Ma<sup>2</sup>, Jianming Bai<sup>1</sup>, Qingping Meng<sup>1</sup>,

Steven N. Ehrlich<sup>1</sup>, Yong-Sheng Hu<sup>2\*</sup>, Xiao-Qing Yang<sup>1\*</sup>

1 Brookhaven National Laboratory, Upton, NY 11973, U.S.A

2 Key Laboratory for Renewable Energy, Beijing Key Laboratory for New Energy  
Materials and Devices, National Laboratory for Condensed Matter Physics, Institute of  
Physics, Chinese academy of Sciences, Beijing, 100190, P.R. China

\*Corresponding author: [yshu@aphy.iphy.ac.cn](mailto:yshu@aphy.iphy.ac.cn); [xyang@bnl.gov](mailto:xyang@bnl.gov)

‡ Xiqian Yu and Huilin Pan contributed equally to this paper

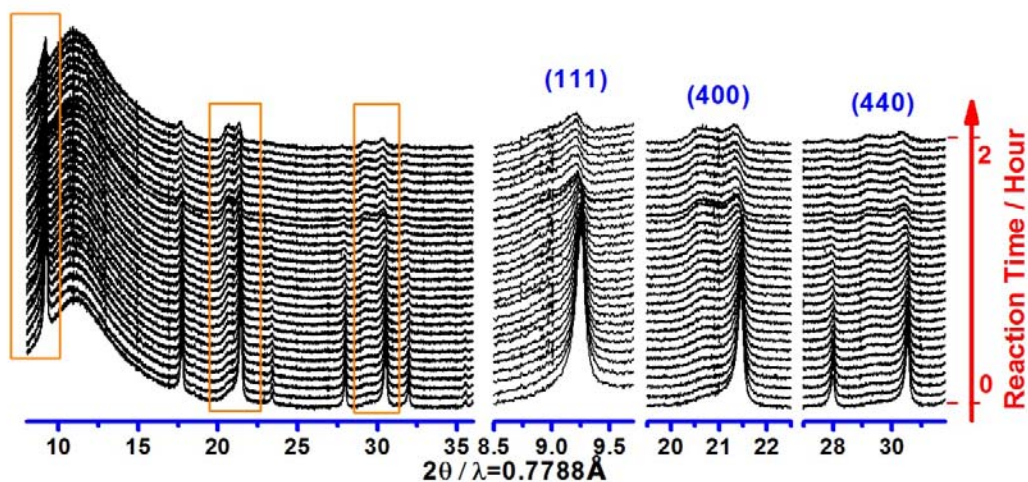


Figure S1 *In situ* XRD patterns collected during chemical sodiation of  $\text{Li}_4\text{Ti}_5\text{O}_{12}$  powder in capillary. The main peaks correspond to (111), (400) and (440) reflections which are highlighted in the right column, respectively. 1 mol Na: 1mol biphenyl per liter DME solution was used as reducing agent.

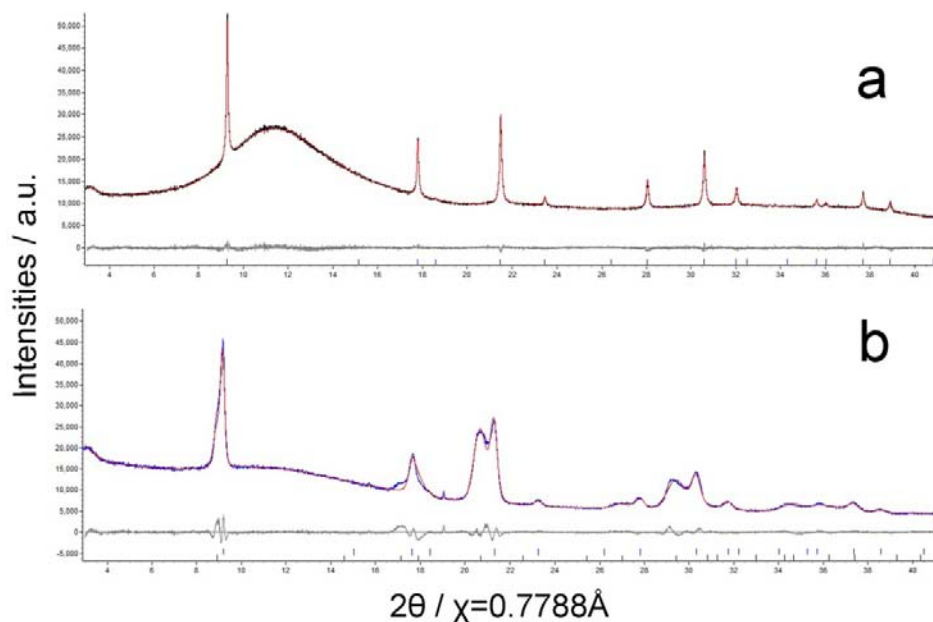


Figure S2 Rietveld refinement of XRD patterns for the pristine (a) and (b) chemically sodiated 44 nm- $\text{Li}_4\text{Ti}_5\text{O}_{12}$  samples. Red, blue, and gray lines correspond to the observed, calculated and difference, respectively.

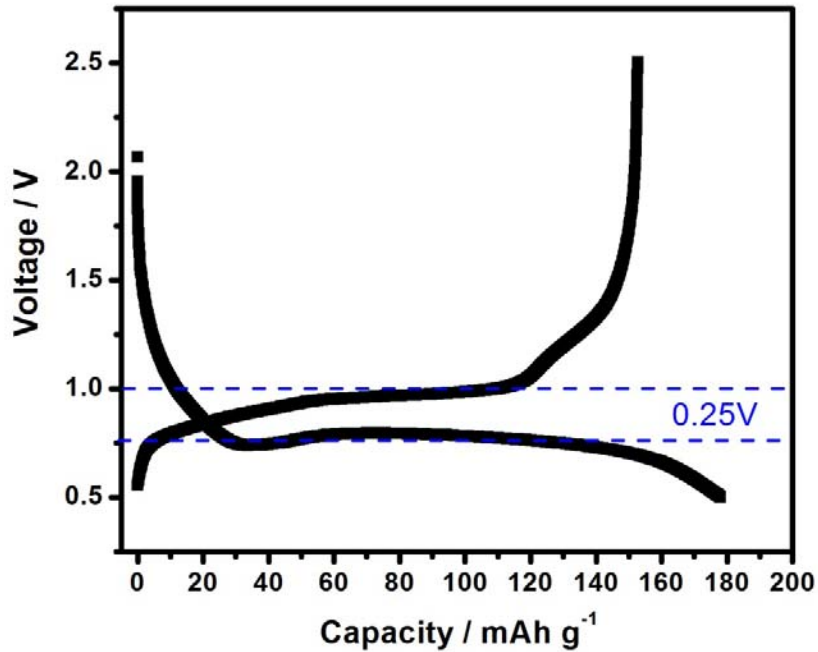


Figure S3 Discharge/charge profile of  $\text{Li}_4\text{Ti}_5\text{O}_{12}/\text{Na}$  cell cycled under a current rate of 0.1C. Large voltage hysteresis can be observed which might be partially contributed with the large strain energy retained within  $\text{Na}_6\text{LiTi}_5\text{O}_{12}$  phase.

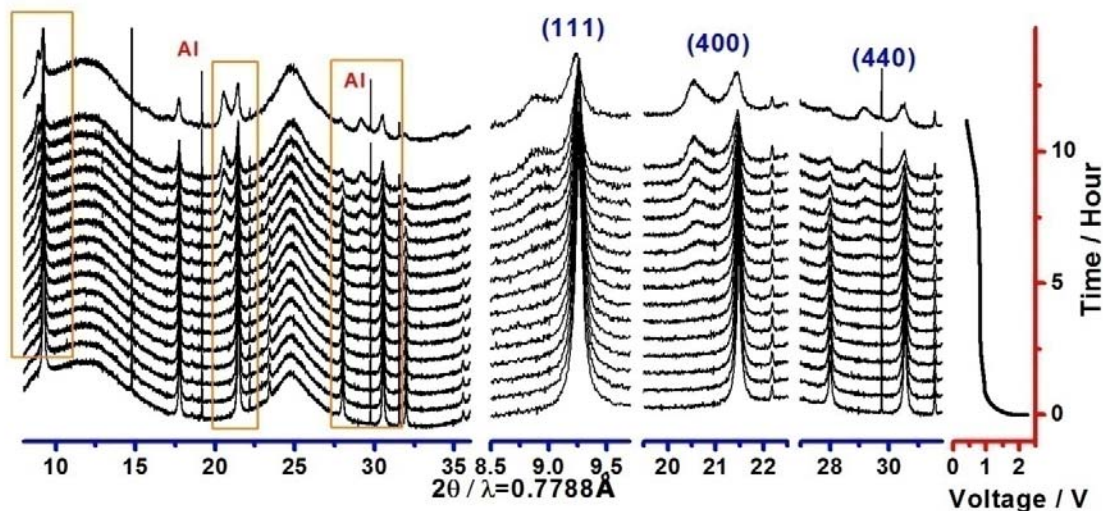


Figure S4 *In situ* XRD patterns collected during first discharge for the  $\text{Li}_4\text{Ti}_5\text{O}_{12}$  electrode in sodium-ion battery system. Each XRD pattern was collected for 15 minutes in order to get better quality. The main peaks correspond to (111), (400) and (440) reflections which are highlighted in the right column, respectively.

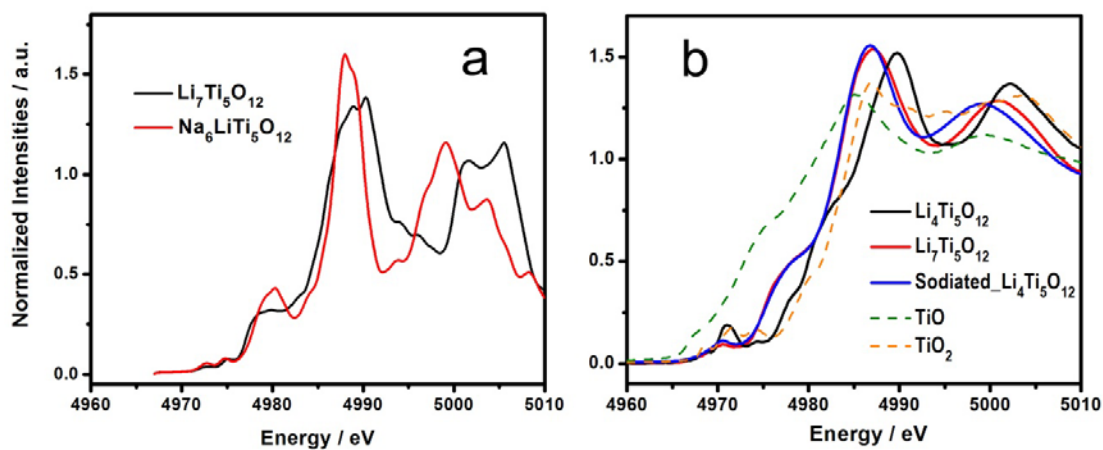


Figure S5 (a) Simulated Ti K-edge spectra of  $\text{Li}_7\text{Ti}_5\text{O}_{12}$  and  $\text{Na}_6\text{LiTi}_5\text{O}_{12}$ , (b) Ti K-edge XANES spectra of  $\text{Li}_4\text{Ti}_5\text{O}_{12}$ ,  $\text{Li}_7\text{Ti}_5\text{O}_{12}$  and sodiated  $\text{Li}_4\text{Ti}_5\text{O}_{12}$ , TiO and  $\text{TiO}_2$  reference spectra were used for comparison.

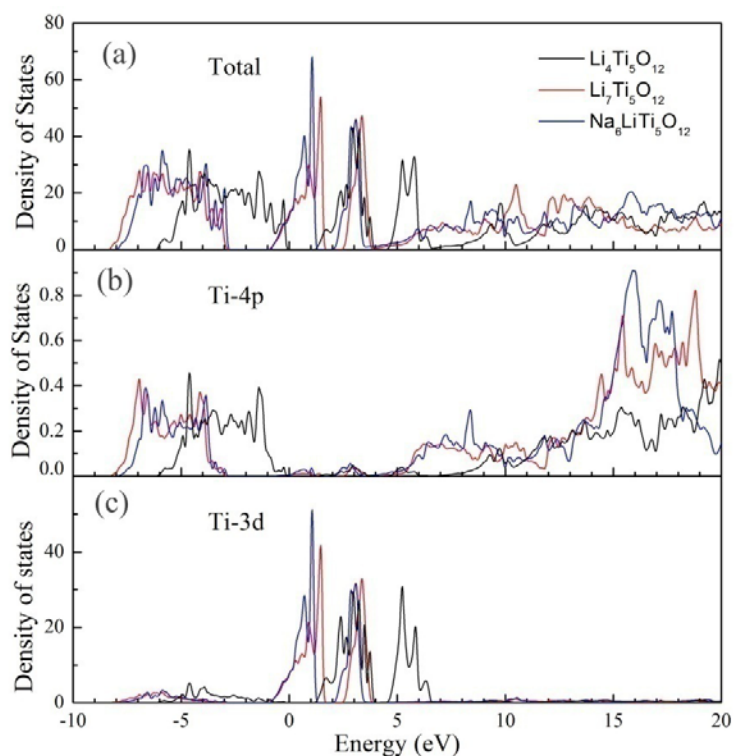


Figure S6 Electronic structure features of the  $\text{Li}_4\text{Ti}_5\text{O}_{12}$ ,  $\text{Li}_7\text{Ti}_5\text{O}_{12}$  and  $\text{Na}_6\text{LiTi}_5\text{O}_{12}$ : Total (a) and projected density of states (DOS) towards Ti-4p (b) and Ti-3d (c) orbitals for  $\text{Li}_4\text{Ti}_5\text{O}_{12}$  (black),  $\text{Li}_7\text{Ti}_5\text{O}_{12}$  (red), and  $\text{Na}_6\text{LiTi}_5\text{O}_{12}$  (blue) calculated by DFT.  $\text{Li}_4\text{Ti}_5\text{O}_{12}$  exhibits insulating behavior with an energy gap of about 1.3 eV, while both  $\text{Li}_7\text{Ti}_5\text{O}_{12}$  and  $\text{Na}_6\text{LiTi}_5\text{O}_{12}$  show metallic behavior. The substitution of Na for Li atoms does not change the Ti-3d DOS around the Fermi level, indicating the same oxidation state of Ti ions in these two compounds. However, because of different ionic radius between  $\text{Na}^+$  and  $\text{Li}^+$  ions, some differences in the electronic structure can still be observed between them, such as narrower bandwidth in  $\text{Na}_6\text{LiTi}_5\text{O}_{12}$ , as evidenced by the Ti-K edge XANES.

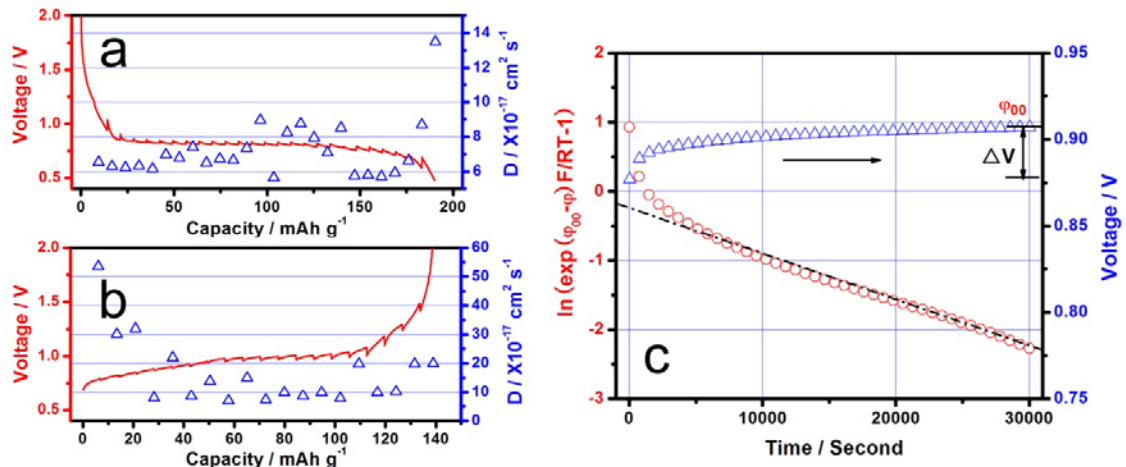


Figure S7 GITT curve and apparent chemical diffusion coefficient curve of the  $\text{Li}_4\text{Ti}_5\text{O}_{12}$ -44 nm|Na cell during (a) discharging and (b) charging; (c) Typical potential relaxation profile of  $\text{Li}_4\text{Ti}_5\text{O}_{12}$ -44 nm sample during GITT experimental when the electrode is discharged to 0.820 V vs.  $\text{Na}^+/\text{Na}$  and corresponding curves of  $\ln[\exp((\phi_{\infty}-\phi)F/RT-1)]$  vs.  $t$ . The dash line indicates the linear fitting result.

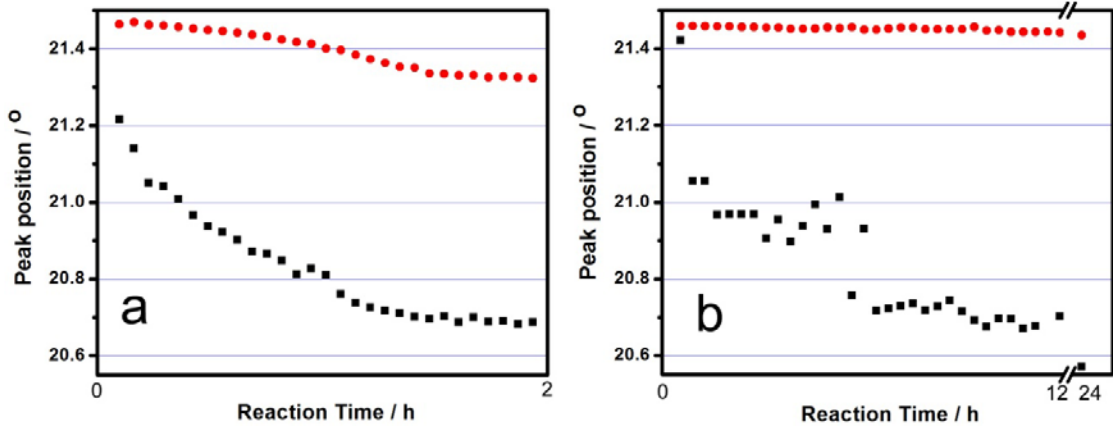


Figure S8 The evolution of (400) peak position of (a) 44 nm and (b) 120 nm  $\text{Li}_4\text{Ti}_5\text{O}_{12}$  with reaction time. Red dot curve:  $\text{Li}_4/\text{Li}_7\text{Ti}_5\text{O}_{12}$ ; Black square curve:  $\text{Na}_6\text{LiTi}_5\text{O}_{12}$ .

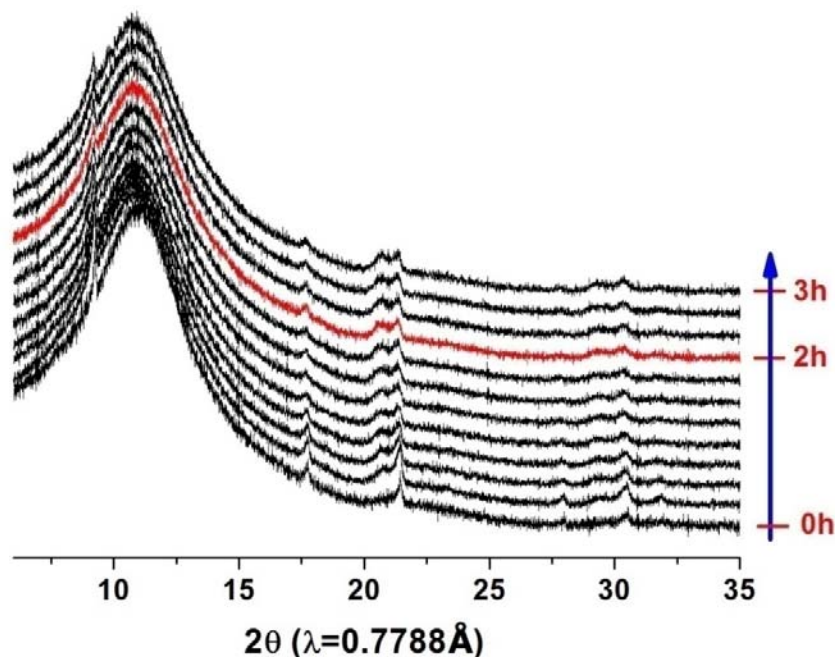


Figure S9 *In situ* XRD patterns collected during chemical sodiation of  $\text{Li}_4\text{Ti}_5\text{O}_{12}$  powder in capillary. 0.8 mol Na:0.8 mol biphenyl per liter DME solution was used as reducing agent.

#### Concentration variation and its impact on the redox potential:

In our typical case, 0.7 mg  $\text{Li}_4\text{Ti}_5\text{O}_{12}$  (1.5  $\mu\text{mol}$ ) was reacted with 9  $\mu\text{mol}$  reducing agent (glass capillary: 0.7 mm in diameter; filled with reducing agent: 2.5 cm in length; total molar value can be calculated as 1.5  $\mu\text{mol}$ ). Reducing agent is overstoichiometric. For simplicity, we assumed the reduction capability comes from the  $\text{C}_{12}\text{H}_{10}^-$  anion, the reduction half-reaction can be written as:  $\text{C}_{12}\text{H}_{10}^- - e^- \rightarrow \text{C}_{12}\text{H}_{10}$ , the corresponding reduction potential can be calculated as  $\varphi = \varphi^0 + 0.0591 \lg \frac{[\text{C}_{12}\text{H}_{10}]}{[\text{C}_{12}\text{H}_{10}^-]}$ ; At the initial state, 1 mol/L Na dissolved in 1 mol/L biphenyl DME solutions. Assuming the dissolved

Na is 0.95 mol/L, then  $[C_{12}H_{10}^-]$  and  $[C_{12}H_{10}]$  are 0.95 mol/L and 0.05 mol/L correspondingly, the reduction potential can be calculated as  $\varphi = \varphi^0 + 0.0591 \lg \frac{0.05}{0.95} = \varphi^0 - 0.076V$ ; After reaction, around half  $C_{12}H_{10}^-$  has been consumed, concentration of the  $C_{12}H_{10}^-$  and  $C_{12}H_{10}$  are close to 1:1, the reduction potential can be calculated as  $\varphi = \varphi^0 + 0.0591 \lg \frac{0.5}{0.5} = \varphi^0$ ; The reduction potential change only 0.076 V after reaction. Therefore, the concentration of the reducing agent would not have much effect during the chemical reaction process.

**Comparison of the apparent diffusion coefficient (D) obtained from chemical and electrochemical Na<sup>+</sup> insertion:**

GITT experiment was performed and the apparent chemical diffusion coefficients regarding discharge and charge are obtained by fitting the voltage relaxation curve based on the diffusion equation<sup>1</sup>:

$$\ln\left[\exp\left(\frac{F}{RT}(\varphi_{\infty} - \varphi) - 1\right)\right] = -\ln N - \frac{4.49^2}{r_0^2} \tilde{D}_{Li} t \quad (1)$$

where the  $\varphi_{\infty}$  is the voltage at equilibrium state and  $r_0$  is the diffusion length for sodium. The apparent diffusion coefficients electrochemically obtained are roughly in the magnitude of  $10^{-16} \sim 10^{-17} \text{ cm}^2 \text{ s}^{-1}$  for sodium insertion, very close to that of  $2.7 \times 10^{-16} \text{ cm}^2 \text{ s}^{-1}$  estimated from chemical process. The apparent diffusion coefficients during Na extraction are in the magnitude of  $\sim 10^{-16}$ , higher than Na insertion.

**Table S1.** Strain and interface contributed thermodynamic driving force

y/R	E(y/R)	$\Delta g(\text{KJ/mol})$	$\Delta V(\text{V})$
0.1	0.34	10.3(0.11)	0.11

0.2	0.58	17.6(0.18)	0.18
0.3	0.76	23.0(0.24)	0.24
0.4	0.86	26.0(0.27)	0.27
0.5	0.92	27.9(0.29)	0.29
0.6	0.95	28.8(0.29)	0.29
0.7	0.97	29.4(0.30)	0.30
0.8	0.98	29.7(0.30)	0.30
0.9	~1	30.3(0.31)	0.31

Table S1 caption

According to Mott and Nabarro's theory,<sup>2</sup> the elastic-strain energy of a spherical inclusion  $\beta$  in matrix  $\alpha$  is

$$\Delta g_{sph} = \frac{2\mu_{\alpha}K_{\beta}}{3K_{\beta} + 4\mu_{\alpha}} \frac{(v_{\beta} - v_{\alpha})^2}{v_{\beta}} \quad (2)$$

where  $\mu_{\alpha}$  is the shear modulus of matrix  $\alpha$ ;  $K_{\beta}$  is bulk modulus of inclusion  $\beta$ ;  $v_{\alpha}$  and  $v_{\beta}$  are respectively the specific volume of  $\alpha$  and  $\beta$  phases. For inclusions with other shape, such as disks, needles etc, the elastic-strain energy<sup>3</sup> is

$$\Delta g_{non-sph} = \Delta g_{sph} E\left(\frac{y}{R}\right) \quad (3)$$

Here  $E\left(\frac{y}{R}\right)$  is a function depended on the inclusion shape.  $R$  and  $y$  represent the semi-axes of a flat oblate spheroid. Although Eshelby<sup>4</sup> proved that the strain energy is entirely independent of the shape if the inclusion has the same rigidity as the matrix, a precipitate of flat sheets is likely to have smaller strain energy than almost any other because the faces of the sheets are nearly free to expand. Using  $E\left(\frac{y}{R}\right)$  value given by Nabarro,<sup>4,5</sup> the

strain energies of various  $\frac{y}{R}$  ratios are calculated. Table S1 shows our calculated results.

Nabarro indicated the strain energy of spherical particle ( $\frac{y}{R} = 1$ ) of precipitate is maximum. Obviously, the results of Table S1 agree with the experimental measurement in magnitude.

[1] Wang, Q.; Li, H.; Huang, X. J.; Chen, L. Q. *J. Electrochem. Soc.* **2001**, *148*, A737.

[2] Mott, N. F.; Nabarro, F. R. N. *Proc. Phys. Soc.* **1940**, *52*, 86.

[3] Eshelby, J. D. *Proc. R. Soc. A*, **1961**, *241*, 376.

[4] Nabarro, F. R. N. *Proc. Phys. Soc.* **1940**, *52*, 90.

[5] Nabarro, F. R. N. *Proc. R. Soc. A*, **1940**, *175*, 519.